

# Early-Terminable Energy-Safe Iterative Coupling for Parallel Simulation of Port-Hamiltonian Systems

Qi Wei, Jianfeng Tao, Hongyu Nie, Wangtao Tan

**Abstract**—Parallel simulation and control of large-scale robotic systems often rely on partitioned time stepping, yet finite-iteration coupling can inject spurious energy by violating power consistency—even when each subsystem is passive. This letter proposes a novel energy-safe, early-terminable iterative coupling for port-Hamiltonian subsystems by embedding a Douglas–Rachford (DR) splitting scheme in scattering (wave) coordinates. The lossless interconnection is enforced as an orthogonal constraint in the wave domain, while each subsystem contributes a discrete-time scattering port map induced by its one-step integrator. Under a discrete passivity condition on the subsystem time steps and a mild impedance-tuning condition, we prove an augmented-storage inequality certifying discrete passivity of the coupled macro-step for any finite inner-iteration budget, with the remaining mismatch captured by an explicit residual. As the inner budget increases, the partitioned update converges to the monolithic discrete-time update induced by the same integrators, yielding a principled, adaptive accuracy–compute trade-off, supporting energy-consistent real-time parallel simulation under varying computational budgets. Experiments on a coupled-oscillator benchmark validate the passivity certificates at numerical roundoff (on the order of  $10e-14$  in double precision) and show that the reported RMS state error decays monotonically with increasing inner-iteration budgets, consistent with the hard-coupling limit.

**Index Terms**—Simulation and Animation, Dynamics, Formal Methods in Robotics and Automation.

## I. INTRODUCTION

THE simulation and control of modern robotic systems increasingly push computation to the limit, as seen in massively parallel learning pipelines [1], [2], high-fidelity simulation of stiff and structurally complex dynamics [3], [4], and microsecond-level latency budgets in high-rate online MPC [5], [6]. These pressures make model partitioning increasingly important for parallel, co-simulation-based execution [7], [8], [9].

Once models are split, the bottleneck becomes the numerical interface: discrete exchange (sample-and-hold, extrapolation, asynchrony, delay) can break power consistency and create coupling defects [10], [11], [12], yielding spurious energy injection (effective negative damping) even when subsystems are passive [10], [13], [14]. An interface must therefore enforce an energy-safe contract, not merely reduce local error.

Related work on partitioned interfaces spans non-iterative (explicit) and iterative schemes [15], [16], [9]: non-iterative zero-order-hold or extrapolation is attractive for real time

but can drift or destabilize under stiff coupling [17], [18], [19], while macro-step iterations (Gauss–Seidel/Jacobi, relaxation) improve consistency [18], [19] but raise delicate finite-iteration stability questions [20]. A distinct class of non-iterative schemes is represented by Transmission Line Modeling (TLM), which exploits physically motivated time delays to decouple subsystems. TLM introduces physically motivated delays to break algebraic loops and preserve passivity [21], [22], [23]. However, fixed delays can distort high-frequency behavior and limit performance [24], [25], [26], motivating delay-free alternatives or impedance tuning.

Structure-preserving modeling makes the interface an explicit power contract: pH/Dirac formulations encode interconnection as a power-conserving constraint [27], [28], [29], and energy-consistent time stepping is well developed for monolithic integration [27], [30], [29] but harder to retain under partitioned, iterative coupling (notably for DAEs and pHDAEs) [31], [29]. In port coordinates the coupling layer is an input–output map whose inequality quantifies equivalent damping; this motivates energy-safe interface updates via operator-splitting compositions [31], [32], whose guarantees are typically asymptotic (or end-of-step), so finite intermediate iterates may still fail to remain physically admissible or passive.

Wave (scattering) variables turn power coupling into passive message passing [33] and are closely related to TLM-style interfaces when explicit delays are introduced [21], [22], [23], [26]. Yet stiff delay-free algebraic loops often still require interface tuning in practice [34], [9], while operator-splitting methods provide asymptotic consistency guarantees but do not by themselves yield a wave-domain, iterate-level energy accounting. This motivates embedding splitting updates in scattering coordinates to obtain parallel coupling with a transparent energy certificate under finite inner iterations.

In this letter, we propose an *anytime* (early-terminable) energy-safe coupling interface by embedding operator-splitting updates in scattering (wave) coordinates. At each macro-step, a Douglas–Rachford (DR) type inner iteration reconciles a lossless wave coupling constraint with the discrete-time port behavior induced by the subsystem integrators, a principled, adaptive accuracy–compute trade-off together with an augmented-storage energy certificate under finite inner iterations. The main contributions are as follows:

- 1) **An anytime energy-safe interface for parallel coupling:** We introduce a parallelizable iterative coupling interface in scattering (wave) variables, using a Douglas–Rachford (DR) inner-loop to enforce the lossless interconnection while remaining energy-safe at every finite iteration (Algorithm 1).
- 2) **Finite-iteration passivity guarantee:** For any finite

Manuscript received January 16, 2026; accepted ;Date of publication ; This work was supported by the National Natural Science Foundation of China (Grant No. 52075320).

The authors are with the School of Mechanical Engineering, Shanghai Jiao Tong University, Shanghai 200240, China. (e-mail: jftao@sjtu.edu.cn)  
Digital Object Identifier

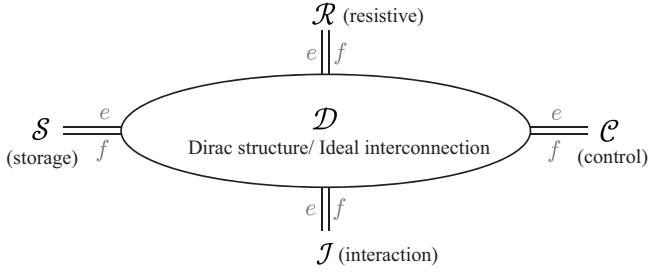


Fig. 1. Port-based view of a pH interconnection. Storage  $\mathcal{S}$ , dissipation  $\mathcal{R}$ , control  $\mathcal{C}$ , and interaction  $\mathcal{J}$  exchange power through port variables  $(e, f)$  and are constrained by a Dirac structure  $\mathcal{D}$ , representing an ideal lossless interconnection ( $e^\top f = 0$ ).

inner-iteration budget, we establish a discrete passivity certificate for the macro-step update via an augmented storage function (Theorem 1).

3) **Convergence to the monolithic discretization:** As the inner-iteration budget increases, the partitioned update provably converges to the monolithic discrete-time update induced by the same integrator, yielding a principled accuracy–compute trade-off (Theorem 2).

The remainder of the letter is organized as follows: Section II states the subsystem and interconnection model; Section III presents the iterative coupling algorithm; Section IV establishes passivity and convergence properties; Section V reports numerical experiments; and Section VI discusses insights, limitations, and future work.

## II. PROBLEM FORMULATION

### A. Port-Hamiltonian Robotic Subsystems

We consider a robotic system decomposed into  $N$  subsystems indexed by  $i \in \{1, \dots, N\}$ , each exchanging power with the rest of the system through a set of power ports.

Let  $x_i(t) \in \mathbb{R}^{n_i}$  denote the state of subsystem  $i$ , and let  $H_i : \mathbb{R}^{n_i} \rightarrow \mathbb{R}$  be a continuously differentiable Hamiltonian representing its stored energy. We model each subsystem in port-Hamiltonian form as

$$\begin{aligned} \dot{x}_i &= (J_i(x_i) - R_i(x_i)) \nabla H_i(x_i) + G_i(x_i) e_i, \\ f_i &= G_i(x_i)^\top \nabla H_i(x_i), \end{aligned} \quad (1)$$

where  $e_i(t) \in \mathbb{R}^{m_i}$  and  $f_i(t) \in \mathbb{R}^{m_i}$  are the port variables (effort and flow),  $G_i$  maps port efforts to state dynamics, and  $J_i, R_i$  encode internal interconnection and dissipation and satisfy

$$J_i(x_i)^\top = -J_i(x_i), \quad R_i(x_i)^\top = R_i(x_i) \succeq 0. \quad (2)$$

The instantaneous power supplied through the ports is given by the standard pairing

$$P_i(t) := e_i(t)^\top f_i(t). \quad (3)$$

Using (1)–(2), the energy balance of subsystem  $i$  satisfies

$$\begin{aligned} \dot{H}_i(x_i) &= \nabla H_i(x_i)^\top (J_i(x_i) - R_i(x_i)) \nabla H_i(x_i) \\ &\quad + \nabla H_i(x_i)^\top G_i(x_i) e_i \\ &\leq e_i^\top f_i, \end{aligned} \quad (4)$$

which is the standard passivity property with storage  $H_i$  and port variables  $(e_i, f_i)$ .

This port abstraction enables modular partitioning and interconnection without exposing internal subsystem coordinates.

### B. Interconnection as Power-Conserving Constraints

Fig.1 summarizes the port-based interconnection view adopted in this letter. To assemble a full robotic system from subsystems, the port variables  $\{(e_i, f_i)\}_{i=1}^N$  are constrained by an interconnection law that enforces power consistency across interfaces. We express such interconnections as algebraic constraints acting only on port variables, without reference to the internal subsystem states.

Let  $e := \text{col}(e_1, \dots, e_N) \in \mathbb{R}^{m_{\text{tot}}}$  and  $f := \text{col}(f_1, \dots, f_N) \in \mathbb{R}^{m_{\text{tot}}}$ , where  $m_{\text{tot}} := \sum_{i=1}^N m_i$  is the total port dimension. The interconnection is described by a set of admissible port pairs

$$(e, f) \in \mathcal{D} \subseteq \mathbb{R}^{m_{\text{tot}}} \times \mathbb{R}^{m_{\text{tot}}}, \quad (5)$$

which we assume to be a linear subspace encoding the network topology and sign conventions. We define *lossless* interconnections as Dirac structures: define the symmetric bilinear form on port pairs by

$$\langle\langle (e, f), (e', f') \rangle\rangle := e^\top f' + e'^\top f, \quad (6)$$

and let  $\mathcal{D}^\perp$  denote the orthogonal complement of  $\mathcal{D}$  with respect to (6). We assume  $\mathcal{D}$  is a (linear) **Dirac structure**, i.e.,

$$\mathcal{D} = \mathcal{D}^\perp. \quad (7)$$

Intuitively, power conservation corresponds to *isotropy* ( $\mathcal{D} \subseteq \mathcal{D}^\perp$ ), while the Dirac condition (7) expresses a *maximal* power-conserving interconnection relation. Consequently, for any  $(e, f) \in \mathcal{D}$ , we have  $0 = \langle\langle (e, f), (e, f) \rangle\rangle = 2e^\top f$ , i.e., **power conservation** at the interconnection level:

$$\langle e, f \rangle := e^\top f = \sum_{i=1}^N e_i^\top f_i = 0, \quad \forall (e, f) \in \mathcal{D}. \quad (8)$$

The key point is that  $\mathcal{D}$  depends only on the coupling architecture and ports, and not on the particular realization of each subsystem; this separation enables modular/parallel subsystem computation subject to  $(e, f) \in \mathcal{D}$ . For convenience, we denote the aggregated port pair by  $z := (e, f)$ . In a time-discretized (implicit) setting, enforcing (1) together with  $(e, f) \in \mathcal{D}$  leads to a globally coupled algebraic system, whereas a partitioned solve requires iterative port-level reconciliation to recover consistency. Our goal is an interconnection iteration that remains anytime energy-safe under a finite inner budget and converges to the monolithic implicit update as the budget increases; in Section III we formulate this as a fixed-point consistency problem in scattering variables.

## III. PASSIVITY-PRESERVING ITERATIVE COUPLING

We design a port-level *interface algorithm* for parallel subsystem solves that preserves lossless power exchange. Fig. 2 illustrates the overall design objective; specifically, our goal is twofold: (i) the interface remains energy-safe

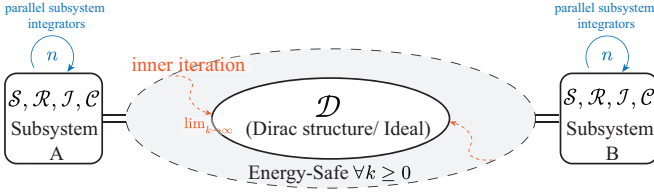


Fig. 2. Parallel iterative coupling of port-Hamiltonian subsystems. A macro-step  $n$  performs parallel subsystem integration; an inner interface iteration enforces an ideal lossless interconnection  $\mathcal{D}$ . The update is energy-safe for any finite number of inner iterations and converges to the monolithic update as the inner iterations increase.

under any finite inner-loop budget, and (ii) increasing the budget drives the update toward the monolithic macro-step. To this end, we combine scattering variables (for norm-preserving power exchange) with a Douglas–Rachford (DR) type splitting (for systematic parallel reconciliation of coupling consistency). We present the two-subsystem case for clarity; the multiport/multisubsystem case follows by stacking the wave variables, with the lossless interconnection represented by an orthogonal coupling matrix  $P$ .

### A. Scattering Representation for Iterative Interconnection

Direct iterations on effort/flow variables  $(e_i, f_i)$  are generally energy-unsafe: intermediate iterates may violate the lossless interconnection constraints and inject spurious energy at the interface. We therefore introduce scattering variables, which provide a power-consistent parametrization and a convenient Euclidean metric for interface signals.

For clarity, we focus on two subsystems  $A$  and  $B$  connected through a common power port of dimension  $m$ , i.e.,  $e_A, f_A, e_B, f_B \in \mathbb{R}^m$ . For each subsystem  $i$ , and for a fixed impedance parameter  $\gamma > 0$ , define the incoming and outgoing wave variables

$$a_i := \frac{e_i + \gamma f_i}{\sqrt{2\gamma}}, \quad b_i := \frac{e_i - \gamma f_i}{\sqrt{2\gamma}}. \quad (9)$$

The inverse relations are

$$e_i = \sqrt{\frac{\gamma}{2}}(a_i + b_i), \quad f_i = \frac{1}{\sqrt{2\gamma}}(a_i - b_i). \quad (10)$$

In these coordinates, the port power takes the form

$$P_i = e_i^\top f_i = \frac{1}{2}(\|a_i\|^2 - \|b_i\|^2), \quad (11)$$

so that the incoming/outgoing wave magnitudes admit a direct power interpretation.

Most importantly, linear lossless interconnections (Dirac structures; Section II-B, (7)) become linear constraints in scattering variables. For example, consider two subsystems  $A$  and  $B$  interconnected by

$$e_A = e_B, \quad f_A + f_B = 0. \quad (12)$$

Substituting (10) yields the wave exchange

$$a_A = b_B, \quad a_B = b_A, \quad (13)$$

i.e., a component swap and therefore norm-preserving (energy-neutral). This observation underlies our scattering-based interface iteration.

### B. Coupling as a Fixed-Point Problem

At each macro time step, interconnection enforcement is a consistency problem between a **lossless coupling constraint** and the **(discrete-time) port behavior** induced by the subsystem integrators. Define the stacked incident/outgoing waves

$$a := \begin{bmatrix} a_A \\ a_B \end{bmatrix} \in \mathbb{R}^{2m}, \quad b := \begin{bmatrix} b_A \\ b_B \end{bmatrix} \in \mathbb{R}^{2m}. \quad (14)$$

For the standard two-subsystem interconnection (12)–(13), the coupling is the swap and can be written as

$$a = Pb, \quad P := \begin{bmatrix} 0 & I \\ I & 0 \end{bmatrix}, \quad P^\top P = I. \quad (15)$$

More generally, we allow any power-preserving coupling  $a = Pb$  with  $P$  orthogonal (covering linear Dirac interconnections; Section II-B, (7)).

At macro-step  $n$ , freeze the subsystem states at  $x_A^n, x_B^n$ . The chosen one-step integrator induces frozen port maps in scattering variables,

$$b_i = S_i^n(a_i), \quad i \in \{A, B\}, \quad (16)$$

and stack them as  $S^n := \text{diag}(S_A^n, S_B^n) : \mathbb{R}^{2m} \rightarrow \mathbb{R}^{2m}$ .

The **monolithic** interface condition at macro-step  $n$  is to find  $(a, b)$  such that both the frozen port relations and the coupling constraint hold:

$$b = S^n(a), \quad a = Pb. \quad (17)$$

Eliminating  $a$  gives the fixed-point equation  $b = S^n(Pb)$  (equivalently,  $a = PS^n(a)$ ), which motivates an inner iteration.

### C. Iterative Coupling Algorithm

We operate on two time scales: a macro-step index  $n$  for subsystem time stepping, and an inner iteration index  $k$  for enforcing port-level coupling consistency. For each subsystem  $i \in \{A, B\}$ , let  $\Phi_i^{\Delta t}$  denote the one-step time-stepping map in scattering variables, i.e.,  $(x_i^{n+1}, b_i^{n+1}) = \Phi_i^{\Delta t}(x_i^n, a_i^n)$ .

At macro-step  $n$ , the one-step integrators induce the frozen scattering port map  $S^n = \text{diag}(S_A^n, S_B^n)$  (16). Define the lifted wave pair  $\zeta := \text{col}(a, b) \in \mathbb{R}^{4m}$  and the coupling subspace

$$\mathcal{C} := \{\zeta = \text{col}(a, b) \in \mathbb{R}^{4m} : a = Pb\},$$

and let  $\Pi_{\mathcal{C}}$  denote the orthogonal projection onto  $\mathcal{C}$  (Remark 1). We enforce coupling consistency via a lifted Douglas–Rachford inner iteration: initialize  $\zeta^{n,0} = \text{col}(a^{n,0}, b^{n,0})$  and for  $k = 0, 1, \dots, K_n - 1$ ,

$$\begin{aligned} (\text{parallel subsystem step}) \quad & \hat{b}^{n,k} := S^n(a^{n,k}), \\ (\text{lift}) \quad & y^{n,k} := \text{col}(a^{n,k}, \hat{b}^{n,k}), \\ (\text{coupling projection}) \quad & \tilde{y}^{n,k} := \Pi_{\mathcal{C}}(2y^{n,k} - \zeta^{n,k}), \\ (\text{DR update}) \quad & \zeta^{n,k+1} := \zeta^{n,k} + \tilde{y}^{n,k} - y^{n,k}. \end{aligned} \quad (18)$$

where  $a^{n,k}$  is the incident-wave block of  $\zeta^{n,k}$ . Let  $\hat{b}^{n,*}$  denote the last available *shadow* from the inner-loop (i.e.,  $\hat{b}^{n,*} := \hat{b}^{n,K_n-1}$  if  $K_n \geq 1$ , and  $\hat{b}^{n,*} := b^{n,0}$  if  $K_n = 0$ ). We then enforce lossless coupling for the macro-step input by setting  $a^n := P\hat{b}^{n,*}$  and recover  $(e_i^n, f_i^n)$  via (10).

---

**Algorithm 1** The proposed iterative coupling algorithm
 

---

**Require:** Initial states  $x_A^0, x_B^0$ ; initial outgoing waves  $b_A^0, b_B^0$ ; time step  $\Delta t$ ; coupling matrix  $P$  with  $P^\top P = I$ ; inner budgets  $K_n$  (and optional tolerance  $\varepsilon > 0$ ).

**Ensure:** For each macro-step  $n$ : updated  $(x_i^{n+1}, b_i^{n+1})$  for  $i \in \{A, B\}$ .

- 1: **for**  $n = 0, 1, 2, \dots$  **do**
- 2: Freeze  $x_A^n, x_B^n$  and form  $S^n = \text{diag}(S_A^n, S_B^n)$  as in (16).
- 3: Initialize  $b^{n,0} \leftarrow \text{col}(b_A^n, b_B^n)$ ,  $a^{n,0} \leftarrow P b^{n,0}$ ,  $\zeta^{n,0} \leftarrow \text{col}(a^{n,0}, b^{n,0})$ , and  $\hat{b}^{n,*} \leftarrow b^{n,0}$ .  
(inner-loop / interface reconciliation)
- 4: **for**  $k = 0, 1, \dots, K_n - 1$  **do**
- 5: Perform one lifted DR step (18) to obtain  $\hat{b}^{n,k}$  and  $\zeta^{n,k+1}$ . ▷ parallel subsystem eval.
- 6:  $\hat{b}^{n,*} \leftarrow \hat{b}^{n,k}$ .
- 7: **if**  $\|\zeta^{n,k+1} - \zeta^{n,k}\| \leq \varepsilon$  **then**
- 8: **break**
- 9: **end if**
- 10: **end for**
- 11: Set coupled incident waves  $a^n \leftarrow P \hat{b}^{n,*}$ .  
(macro-step / parallel subsystem solve)
- 12: **for all**  $i \in \{A, B\}$  **do** ▷ in parallel
- 13:  $(x_i^{n+1}, b_i^{n+1}) \leftarrow \Phi_i^{\Delta t}(x_i^n, a_i^n)$ .
- 14: **end for**
- 15: **end for**

---

*Remark 1* (Closed-form coupling projection). For the linear constraint  $a = Pb$  with  $P^\top P = I$ , the projection  $\Pi_C$  admits a closed form. In particular, for any  $\hat{a}, \hat{b} \in \mathbb{R}^{2m}$ ,

$$\Pi_C(\text{col}(\hat{a}, \hat{b})) = \text{col}(P\bar{b}, \bar{b}), \quad \bar{b} := \frac{1}{2}(\hat{b} + P^\top \hat{a}).$$

Thus the coupling update is closed-form and inexpensive.

*Remark 2* (Connection to explicit interfaces). The limit case  $K_n = 0$  (skipping the inner-loop) reduces to the explicit scattering interface  $a^n = P \text{col}(b_A^n, b_B^n)$ .

Each inner step evaluates  $S_A^n$  and  $S_B^n$  in parallel, and the coupling update is a small closed-form linear operation.

#### D. Energy Interpretation

Wave variables provide a direct energy accounting: by (11),  $P_i = \frac{1}{2}(\|a_i\|^2 - \|b_i\|^2)$ . Since  $P$  is orthogonal, the coupling step  $a = Pb$  is energy-neutral; thus any net energy behavior in the inner-loop is due solely to the mismatch between the frozen port relation  $b = S^n(a)$  and the coupling constraint.

### IV. PASSIVITY AND CONVERGENCE PROPERTIES

This section establishes two main properties of the proposed iterative coupling. Under any *finite* inner-iteration budget, the coupled macro-step update is energy-safe (discrete-passive) in an augmented-storage sense (Theorem 1). Moreover, as the inner-iteration budget increases, the resulting partitioned update converges to the monolithic discrete-time update induced by the same subsystem integrators (Theorem 2). We start from two standing conditions: an energy-safe subsystem integrator (Condition 1) and firm nonexpansiveness (resolvent form) of the frozen port maps (Condition 2).

#### A. Setup and Standing Conditions

We work in finite-dimensional Euclidean spaces and use standard properties of firmly nonexpansive maps (resolvent representation) and Douglas–Rachford splitting (DRS). For two subsystems with port dimension  $m$ , define stacked waves  $a = \text{col}(a_A, a_B) \in \mathbb{R}^{2m}$  and  $b = \text{col}(b_A, b_B) \in \mathbb{R}^{2m}$ , and define the stacked wave pair

$$\zeta := \text{col}(a, b) \in \mathbb{R}^{4m}, \quad \|\zeta\|^2 := \|a\|^2 + \|b\|^2. \quad (19)$$

To avoid confusion with Section II (where  $z := (e, f)$  denotes an effort/flow port pair), we reserve  $\zeta$  for wave pairs. Let the lossless coupling be  $a = Pb$  with  $P^\top P = I$  (the scattering-domain representation of a linear Dirac interconnection; Section II-B, (7)), and define the associated linear subspace

$$\mathcal{C} := \{\zeta = \text{col}(a, b) \in \mathbb{R}^{4m} : a = Pb\}. \quad (20)$$

At macro-step  $n$ , the chosen one-step integrator induces frozen port maps  $S_i^n : a_i \mapsto b_i$  and  $S^n = \text{diag}(S_A^n, S_B^n)$  as in (16).

**Condition 1** (Energy-safe subsystem integrator). *For each  $i \in \{A, B\}$ , the discrete-time update map  $\Phi_i^{\Delta t}$  satisfies, for all  $n$ ,*

$$H_i(x_i^{n+1}) - H_i(x_i^n) \leq \frac{1}{2}(\|a_i^n\|^2 - \|b_i^{n+1}\|^2), \quad (21)$$

where  $a_i^n$  is the incident wave used to advance subsystem  $i$  over the macro-step and  $b_i^{n+1}$  is the resulting outgoing wave.

*Remark 3* (Passivity-preserving integrators satisfy Condition). Many passivity-preserving one-step methods for port-Hamiltonian systems enforce (21) in scattering coordinates by construction; here we simply treat (21) as a standing *condition* on the chosen subsystem integrators.

**Condition 2** (Frozen port maps are resolvents (FNE)). *At each macro-step  $n$ , each frozen port map  $S_i^n : \mathbb{R}^m \rightarrow \mathbb{R}^m$  is firmly nonexpansive (FNE) in the Euclidean norm:*

$$\|S_i^n(\alpha) - S_i^n(\beta)\|^2 \leq \langle S_i^n(\alpha) - S_i^n(\beta), \alpha - \beta \rangle, \quad (22)$$

$$\forall \alpha, \beta \in \mathbb{R}^m.$$

In our scattering implementation, this property is enforced by a suitable choice of the impedance parameter  $\gamma$ ; see Proposition 1.

**Proposition 1** (A sufficient  $\gamma$ -rule for FNE (impedance bound)). *Fix  $n$  and a subsystem  $i \in \{A, B\}$ . Suppose the frozen discrete-time incremental port relation induced by the chosen one-step integrator can be written as*

$$\delta e_i = Z_{i,d}^n \delta f_i,$$

with a symmetric matrix  $Z_{i,d}^n \succeq 0$ . Let  $S_i^n$  denote the induced frozen wave map for scattering impedance  $\gamma > 0$ . If  $Z_{i,d}^n \succeq \gamma I$ , then  $S_i^n$  is firmly nonexpansive (hence Condition 2 holds for subsystem  $i$  at macro-step  $n$ ).

*Proof.* With the scattering transform  $a = (e + \gamma f)/\sqrt{2\gamma}$  and  $b = (e - \gamma f)/\sqrt{2\gamma}$ , increments satisfy  $\delta a = \frac{1}{\sqrt{2\gamma}}(Z_{i,d}^n + \gamma I)\delta f_i$  and  $\delta b = \frac{1}{\sqrt{2\gamma}}(Z_{i,d}^n - \gamma I)\delta f_i$ , hence

$$\delta b = (Z_{i,d}^n - \gamma I)(Z_{i,d}^n + \gamma I)^{-1} \delta a.$$

If  $Z_{i,d}^n \succeq \gamma I$ , then for every eigenvalue  $\lambda \geq \gamma$  of  $Z_{i,d}^n$  the corresponding eigenvalue of  $S_i^n$  is  $(\lambda - \gamma)/(\lambda + \gamma) \in [0, 1]$ , so  $0 \preceq S_i^n \preceq I$ . A self-adjoint linear map with spectrum in  $[0, 1]$  is firmly nonexpansive [35].  $\square$

*Remark 4* ( $\gamma$  as a tuning parameter). Condition 2 is a property of the *discrete-time* frozen port map and depends on the scattering impedance  $\gamma$ . Proposition 1 provides a conservative rule: selecting  $\gamma$  below a uniform lower bound on the incremental discrete impedance (e.g.,  $\gamma \leq \inf_n \lambda_{\min}(Z_{i,d}^n)$  on the relevant trajectory set) guarantees FNE. In practice, (22) can be monitored via the empirical margin  $\Delta$  used in Section V; persistent negative margins indicate that the chosen  $(\gamma, \Delta t)$  violates Condition 2. In the linear symmetric-impedance case, the bound  $Z_{i,d}^n \succeq \gamma I$  is also *necessary*, hence if-and-only-if.

### B. Discrete Passivity under Finite Iterations

Fix a macro-step  $n$  and consider the inner-loop of Section III-C. We make explicit the distinction between the *DR iterate* (the object to which standard DRS theorems apply) and the *coupling-consistent interface signal* used to drive the macro-step update.

Let  $\zeta^{n,*} \in \mathcal{C}$  denote a *monolithic* interface solution at macro-step  $n$  (not necessarily unique), i.e., a wave pair satisfying the coupling constraint and the frozen subsystem relations:

$$\zeta^{n,*} = \text{col}(a^{n,*}, b^{n,*}) \in \mathcal{C}, \quad b^{n,*} = S^n(a^{n,*}). \quad (23)$$

Here “monolithic” means: for the *same* discrete-time integrators used to define  $S_i^n$  at macro-step  $n$ , both  $a = Pb$  and  $b = S^n(a)$  hold simultaneously.

Under Condition 2,  $S^n$  is firmly nonexpansive; hence there exists a maximal monotone operator  $A^n$  on  $\mathbb{R}^{2m}$  such that  $S^n = J_{A^n} := (I + A^n)^{-1}$  [35]. Eliminating  $a = Pb$  in (23) yields the reduced macro-step interface condition for the stacked outgoing wave  $b := \text{col}(b_A, b_B) \in \mathbb{R}^{2m}$ :

$$0 \in A^n(b) + (I - P)b. \quad (24)$$

Thus, at macro-step  $n$  the interface solve reduces to finding a zero of the sum of two maximal monotone operators, for which DRS applies. This reduced-coordinate DRS is algebraically equivalent to the lifted iteration (18), while being more convenient for analysis. Let  $L := I - P$ , whose resolvent is  $J_L = (I + L)^{-1} = (2I - P)^{-1}$ .

*Remark 5* (Monotonicity of the linear coupling operator). For any orthogonal  $P$ , the linear map  $L := I - P$  is monotone since  $\langle x, Lx \rangle = \|x\|^2 - \langle x, Px \rangle \geq \|x\|^2 - \|x\|\|Px\| = 0$ , hence maximal monotone [35].

We now describe the DR iterate and its shadow. The variable  $u^{n,k}$  is the DR iterate (an auxiliary trial input to the port map). Its *shadow*  $\hat{b}^{n,k} := J_{A^n}(u^{n,k})$  yields a coupling-consistent incident wave  $\hat{a}^{n,k} = P\hat{b}^{n,k}$ , which is the interface signal used to drive the macro-step update. Initialize  $u^{n,0} \in \mathbb{R}^{2m}$  and generate the DRS iterates for (24):

$$\begin{aligned} \hat{b}^{n,k} &:= J_{A^n}(u^{n,k}) = S^n(u^{n,k}), \\ v^{n,k} &:= J_L(2\hat{b}^{n,k} - u^{n,k}), \\ u^{n,k+1} &:= u^{n,k} + v^{n,k} - \hat{b}^{n,k}. \end{aligned} \quad (25)$$

Equivalently, (25) defines a DRS operator  $T_{\text{DR}}^n$  via  $u^{n,k+1} = T_{\text{DR}}^n(u^{n,k})$ . The coupling-consistent wave pair associated with  $\hat{b}^{n,k}$  is

$$\zeta^{n,k} := \text{col}(P\hat{b}^{n,k}, \hat{b}^{n,k}) \in \mathcal{C}, \quad \hat{a}^{n,k} := P\hat{b}^{n,k}. \quad (26)$$

In Algorithm 1, the subsystems are advanced once using  $\hat{a}^n := P\hat{b}^{n,*}$ , where  $\hat{b}^{n,*}$  denotes the last available shadow.

Define the **augmented storage** at macro-step  $n$  (relative to the monolithic interface solution) as

$$\mathcal{V}^n := H_A(x_A^n) + H_B(x_B^n) + \frac{1}{2}\|u^{n,K_n} - u^{n,\dagger}\|^2, \quad (27)$$

where  $u^{n,\dagger} \in \text{Fix}(T_{\text{DR}}^n)$  is a fixed point of the DRS operator associated with (25) (equivalently,  $J_{A^n}(u^{n,\dagger}) = b^{n,*}$  is a monolithic interface solution). The additional term quantifies the inner-loop fixed-point residual and accounts for finite interface mismatch. Since  $J_{A^n}$  is firmly nonexpansive, the Fejér decrease of  $\|u^{n,k} - u^{n,\dagger}\|$  also controls the shadow mismatch  $\|\hat{b}^{n,k} - b^{n,*}\|$ .

**Theorem 1** (Energy safety under finite inner iterations). *Suppose Condition 1 holds and the inner iteration (25) is executed for  $K_n$  steps at macro-step  $n$ , and the macro-step update is driven by  $\hat{a}^n := P\hat{b}^{n,*}$ , where  $\hat{b}^{n,*}$  denotes the last available shadow. Under Condition 2 and the solvability condition that  $\zeta^{n,*}$  exists, the coupled macro-step update satisfies the inequality*

$$\begin{aligned} &(H_A(x_A^{n+1}) + H_B(x_B^{n+1})) - (H_A(x_A^n) + H_B(x_B^n)) \\ &\quad + \frac{1}{2}\|u^{n,K_n} - u^{n,\dagger}\|^2 - \frac{1}{2}\|u^{n,0} - u^{n,\dagger}\|^2 \\ &\leq \frac{1}{2}(\|\hat{a}^n\|^2 - \|b^{n+1}\|^2). \end{aligned} \quad (28)$$

*In particular, any finite inner-loop mismatch is accounted for by the decrease of the DRS fixed-point residual term  $\frac{1}{2}\|u^{n,k} - u^{n,\dagger}\|^2$  (a Fejér-monotone quantity), while the physical energy change is controlled by the supplied wave power.*

Here  $b^{n+1}$  denotes the actual outgoing wave produced by advancing the subsystems once with input  $\hat{a}^n$ .

If  $K_n = 0$ , we take  $\hat{b}^{n,*} = b^{n,0}$ .

*Proof.* Fix  $n$ . Under Condition 2,  $S^n$  is firmly nonexpansive and hence there exists a maximal monotone operator  $A^n$  such that  $S^n = J_{A^n}$  [35]. Define  $L := I - P$ ; by Remark 5,  $L$  is maximal monotone. Let  $R_{A^n} := 2J_{A^n} - I$  and  $R_L := 2J_L - I$ ; since resolvents are firmly nonexpansive, the reflections are nonexpansive and the Douglas–Rachford operator

$$T_{\text{DR}}^n := \frac{1}{2}(I + R_L R_{A^n})$$

is firmly nonexpansive [35]. Since  $u^{n,k+1} = T_{\text{DR}}^n(u^{n,k})$ , firm nonexpansiveness implies Fejér monotonicity of the Picard iterates with respect to  $\text{Fix}(T_{\text{DR}}^n)$  [35]: for any  $u^{n,\dagger} \in \text{Fix}(T_{\text{DR}}^n)$ ,

$$\|u^{n,k+1} - u^{n,\dagger}\|^2 \leq \|u^{n,k} - u^{n,\dagger}\|^2, \quad \forall k.$$

In particular,  $\|u^{n,K_n} - u^{n,\dagger}\|^2 - \|u^{n,0} - u^{n,\dagger}\|^2 \leq 0$ .

Next, apply Condition 1 to the macro-step update driven by  $\hat{a}^n$  and sum over  $i \in \{A, B\}$ :

$$\begin{aligned} &(H_A(x_A^{n+1}) + H_B(x_B^{n+1})) - (H_A(x_A^n) + H_B(x_B^n)) \\ &\leq \frac{1}{2}(\|\hat{a}^n\|^2 - \|b^{n+1}\|^2). \end{aligned}$$

Finally, add the Fejér decrease to obtain (28).  $\square$

### C. Hard-Coupling Limit Recovers the Monolithic Update

We next formalize the hard-coupling limit claim: as  $K_n \rightarrow \infty$ , the inner loop makes the shadow interface signal converge to a monolithic interface, and the resulting partitioned macro-step recovers the monolithic discrete-time update induced by the same discretization. In this subsection we additionally assume continuity of the one-step maps in the incident wave input (and continue to assume solvability of the monolithic interface condition, i.e., existence of  $\zeta^{n,*}$ ).

**Lemma 1** (Inner-loop convergence to the monolithic interface). *Under Condition 2 and the solvability condition that  $\zeta^{n,*}$  exists, the DRS iterates  $u^{n,k}$  in (25) converge to a fixed point  $u^{n,\dagger} \in \text{Fix}(T_{\text{DR}}^n)$ , and the shadow sequence  $\hat{b}^{n,k} := J_{A^n}(u^{n,k})$  converges to a monolithic outgoing wave  $b^{n,*}$  solving (24). Consequently,  $\hat{a}^{n,k} = P\hat{b}^{n,k}$  converges to  $a^{n,*} = Pb^{n,*}$ .*

*Proof.* Under Condition 2,  $S^n = J_{A^n}$  for some maximal monotone  $A^n$  [35]. By Remark 5,  $L := I - P$  is maximal monotone. The standard Douglas–Rachford splitting convergence theory for sums of maximal monotone operators therefore applies [36], [37], yielding convergence of the DR iterates to a fixed point and convergence of the shadow to a solution; in finite dimension, weak and strong convergence coincide.  $\square$

**Theorem 2** (Hard-coupling limit recovers the monolithic discretization). *Assume Lemma 1 holds at each macro-step  $n$ , and assume the one-step update maps  $\Phi_i^{\Delta t}$  are continuous in their arguments  $(x_i^n, a_i^n)$  on the relevant set of trajectories. Then, for any fixed finite horizon  $T = N\Delta t$ , if  $K_n \rightarrow \infty$  for each  $n = 0, \dots, N - 1$ , the partitioned trajectory produced by Algorithm 1 converges (step-by-step on the grid) to a monolithic discrete-time trajectory obtained by selecting a solution of (23) at each macro-step.*

*Proof.* Fix a finite horizon  $T = N\Delta t$ . For each macro-step  $n \in \{0, \dots, N - 1\}$ , Lemma 1 gives  $\hat{b}^{n,*} \rightarrow b^{n,*}$  (hence  $\hat{a}^n = P\hat{b}^{n,*} \rightarrow a^{n,*}$ ) as  $K_n \rightarrow \infty$ . By continuity of  $\Phi_i^{\Delta t}$  and induction on  $n$ , the one-step update  $(x_i^{n+1}, b_i^{n+1}) = \Phi_i^{\Delta t}(x_i^n, \hat{a}^n)$  converges to the monolithic update at step  $n$ , yielding grid-pointwise convergence of the partitioned trajectory to the monolithic discrete-time trajectory over the horizon.  $\square$

*Remark 6* (Nonuniqueness and solution selection). If (23) admits multiple solutions at a macro-step, then the limiting interface/trajectory in the hard-coupling limit may depend on initialization and implicit selection by the inner iteration. Theorem 2 guarantees convergence to a trajectory consistent with *some* solution selection; explicit selection mechanisms are left for future work (Section VI).

## V. EXPERIMENTS: TWO-OSCILLATOR BENCHMARK

We validate the iterative coupling framework on a minimal yet nontrivial benchmark: two coupled oscillators split into two subsystems with one scattering port each. Nontriviality comes from a *mixed Duffing–linear* configuration: Subsystem A includes a stiff hardening spring nonlinearity, so the frozen discrete-time port maps are state-dependent and cannot be reduced to a globally linear impedance bound. The experiments

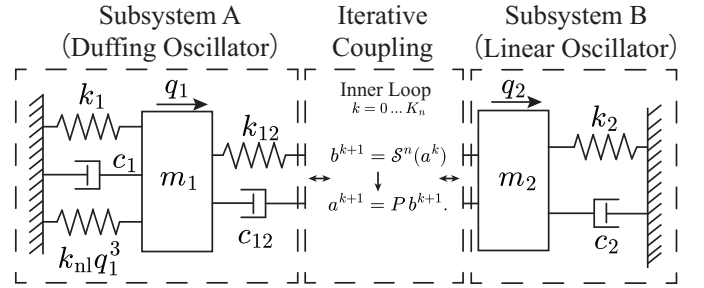


Fig. 3. Schematic of the two-oscillator benchmark.

TABLE I  
TWO-OSCILLATOR BENCHMARK PARAMETERS AND SIMULATION SETTINGS.

Parameter	Value	Parameter	Value
$m_1$	8.0	$m_2$	4.0
$k_1$	100	$k_2$	50
$c_1$	0	$c_2$	0
$k_{12}$	120	$c_{12}$	0.05
$k_{\text{nl}}$	8000	$q_1(0)$	0.4
$q_2(0)$	0	$v_1(0) = v_2(0)$	0
$\Delta t$	0.01	$T$	10.0
$\gamma$	0.4	$K_n$	{0, 3, 8, 20, 35, 50}

target three claims from Sections III–IV: (i) Condition 2 (FNE margins), (ii) the augmented-storage energy certificate under finite inner iterations (Theorem 1), and (iii) convergence to a monolithic reference trajectory as  $K_n \rightarrow \infty$  (Theorem 2).

### A. Benchmark and settings.

Fig. 3 depicts the subsystem decomposition and ports. Each subsystem exposes a single port  $(e_i, f_i)$  and is interfaced through scattering variables  $(a_i, b_i)$  (Section III-A); lossless coupling is enforced via  $a = Pb$  with  $P$  the swap matrix (Section III-B). Both subsystems are time-discretized by a passivity-preserving, energy-consistent discrete-gradient one-step method, so Condition 1 holds by construction; for the linear subsystem, this reduces to an implicit midpoint/trapezoidal update. All model and simulation parameters are listed in Table I.

For the Duffing subsystem we treat  $\gamma$  as a design parameter (Table I) and verify Condition 2 numerically via the FNE margins reported in Fig. 5(a). Since the hardening Duffing spring has amplitude-dependent incremental stiffness  $\Delta F/\Delta q$  (due to the cubic term), the induced incremental behavior is state-dependent; thus we do not claim a trajectory-independent guarantee and instead verify Condition 2 along the realized trajectories using a finite set of test pairs.

### B. Results and analysis.

Fig. 4 compares the trajectories  $q_1(t)$  and  $q_2(t)$  for different inner-iteration budgets  $K_n$  against a monolithic reference computed with the same passivity-preserving discrete-gradient time stepper and time step  $\Delta t$ .

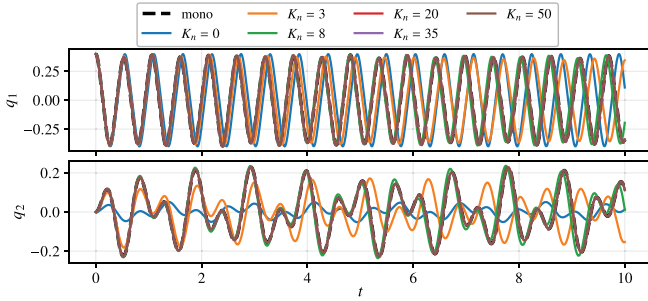


Fig. 4. Trajectories  $(q_1, q_2)$  for different inner-iteration budgets  $K_n$  and the monolithic reference.

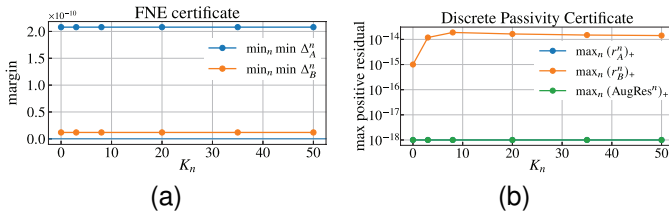


Fig. 5. Two-oscillator certificates versus inner-iteration budget  $K_n$ . (a) FNE certificate: worst-case numerically evaluated margins for Condition 2. (b) Discrete-passivity and augmented-storage diagnostics: positive-part summaries  $(\cdot)_+$  of the discrete-passivity residual (21) and the augmented-storage residual associated with (28).

We check Condition 2 at each macro-step  $n$  by freezing subsystem states when evaluating  $S_i^n$  and estimating the margin induced by (22) on a finite set of test pairs  $(\alpha, \beta)$ .

$$\Delta_i^n(\alpha, \beta) := \langle S_i^n(\alpha) - S_i^n(\beta), \alpha - \beta \rangle - \|S_i^n(\alpha) - S_i^n(\beta)\|^2, \quad (29)$$

so (22) holds iff  $\Delta_i^n(\alpha, \beta) \geq 0$  for all  $\alpha, \beta$ . Fig. 5(a) reports  $\min_n \min \Delta_i^n$  and the number of test pairs with  $\Delta_i^n < -\text{tol}$  ( $\text{tol} = 10^{-12}$ ) for each inner-iteration budget; since the trajectory depends on  $K_n$ , these margins also vary with  $K_n$ .

For discrete passivity, we monitor the residual induced by (21),  $r_i^n := (H_i(x_i^{n+1}) - H_i(x_i^n)) - \frac{1}{2}(\|a_i^n\|^2 - \|b_i^{n+1}\|^2)$ , so Condition 1 holds at step  $n$  whenever  $r_i^n \leq 0$ ; Fig. 5(b) summarizes  $(r_i^n)_+$ , together with the positive part of the *augmented-storage residual* associated with (28) (Theorem 1), i.e., the quantity obtained by moving the right-hand side to the left.

Finally, Fig. 6 shows that the reported RMS state error to the monolithic reference decreases monotonically over the tested budgets as  $K_n$  increases, consistent with Theorem 2.

In summary, for the selected  $\gamma$ , the FNE margins along the realized trajectories are numerically nonnegative (Fig. 5(a)), indicating that Condition 2 is consistent with the benchmark. The discrete-passivity residuals and the augmented-storage residual are essentially nonpositive in the reported positive-part summaries (Fig. 5(b)), with any remaining positive part at numerical roundoff (on the order of  $10^{-14}$  in double precision), supporting the finite-iteration certificate of Theorem 1. Finally, increasing  $K_n$  monotonically reduces the reported RMS state error and approaches the monolithic reference (Fig. 6), consistent with Theorem 2.

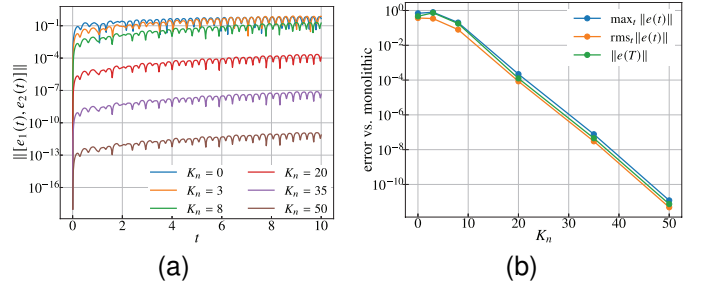


Fig. 6. Hard-coupling limit validation (Theorem 2). (a) RMS state error versus time relative to the monolithic reference. (b) RMS error decay versus  $K_n$  (monotonic over the tested budgets).

## VI. DISCUSSION

This letter frames iterative coupling of port-Hamiltonian subsystems as a *numerical interface design* problem solved by a Douglas–Rachford inner iteration in scattering coordinates. The resulting augmented-storage inequality provides an *any-time* (early-terminable) energy-safety certificate for any finite inner-iteration budget, while the hard-coupling limit recovers the monolithic discrete-time update induced by the same subsystem integrators. Viewed as an explicit interface layer, the inner-iteration budget becomes an adjustable knob for an adaptive accuracy–compute trade-off, supporting energy-consistent real-time parallel simulation under varying computational budgets. The scattering-domain formulation also resembles passive message passing, suggesting a composable route to distributed co-simulation and in-the-loop, large-scale model-based optimization/control workflows in which subsystems are evaluated in parallel while coupling consistency is reconciled with a certificate. More broadly, this perspective shifts interface stabilization from ad-hoc tuning heuristics toward certificate-driven numerical interface design grounded in operator splitting. Open directions include quantitative finite- $K_n$  state-error bounds, explicit solution selection when the monolithic interface admits multiple solutions, and adaptive impedance/budget selection (including asynchronous and communication-aware extensions).

## REFERENCES

- [1] N. Rudin, D. Hoeller, P. Reist, and M. Hutter, “Learning to walk in minutes using massively parallel deep reinforcement learning,” in *Conference on robot learning*. PMLR, 2022, pp. 91–100.
- [2] V. Makoviychuk, L. Wawrzyniak, Y. Guo, M. Lu, K. Storey, M. Macklin, D. Hoeller, N. Rudin, A. Allshire, A. Handa *et al.*, “Isaac gym: High performance gpu-based physics simulation for robot learning,” *arXiv preprint arXiv:2108.10470*, 2021.
- [3] E. Todorov, T. Erez, and Y. Tassa, “Mujoco: A physics engine for model-based control,” in *2012 IEEE/RSJ international conference on intelligent robots and systems*. IEEE, 2012, pp. 5026–5033.
- [4] Y. Hu, L. Anderson, T.-M. Li, Q. Sun, N. Carr, J. Ragan-Kelley, and F. Durand, “DiffTaichi: Differentiable programming for physical simulation,” *arXiv preprint arXiv:1910.00935*, 2019.
- [5] R. Grandia, F. Jenelten, S. Yang, F. Farshidian, and M. Hutter, “Perceptive locomotion through nonlinear model-predictive control,” *IEEE Transactions on Robotics*, vol. 39, no. 5, pp. 3402–3421, 2023.
- [6] T. Salzmann, E. Kaufmann, J. Arrizabalaga, M. Pavone, D. Scaramuzza, and M. Ryll, “Real-time neural mpc: Deep learning model predictive control for quadrotors and agile robotic platforms,” *IEEE Robotics and Automation Letters*, vol. 8, no. 4, pp. 2397–2404, 2023.

- [7] D. Negrut, R. Serban, H. Mazhar, and T. Heyn, "Parallel computing in multibody system dynamics: why, when, and how," *Journal of Computational and Nonlinear Dynamics*, vol. 9, no. 4, p. 041007, 2014.
- [8] A. V. Papadopoulos and A. Leva, "A model partitioning method based on dynamic decoupling for the efficient simulation of multibody systems," *Multibody System Dynamics*, vol. 34, no. 2, pp. 163–190, 2015.
- [9] B. Schweizer, P. Li, and D. Lu, "Explicit and implicit cosimulation methods: stability and convergence analysis for different solver coupling approaches," *Journal of Computational and Nonlinear Dynamics*, vol. 10, no. 5, p. 051007, 2015.
- [10] S. Sadjina, L. T. Kyllingstad, E. Pedersen, and S. Skjong, "Energy conservation and co-simulation: Background and challenges," in *Proceedings of the 2024 International Conference on Bond Graph Modeling and Simulation (ICBGM'24)(San Diego, CA, USA, 1st–3rd July 2024)*, 2024.
- [11] S. Sadjina, L. T. Kyllingstad, S. Skjong, and E. Pedersen, "Energy conservation and power bonds in co-simulations: non-iterative adaptive step size control and error estimation," *Engineering with Computers*, vol. 33, no. 3, pp. 607–620, 2017.
- [12] M. Benedikt, D. Watzenig, J. Zehetner, and A. Hofer, "Nepce-a nearly energy-preserving coupling element for weak-coupled problems and co-simulations," in *COUPLED V: proceedings of the V International Conference on Computational Methods for Coupled Problems in Science and Engineering*. CIMNE, 2013, pp. 1021–1032.
- [13] F. González, S. Arbatani, A. Mohtat, and J. Kövecses, "Energy-leak monitoring and correction to enhance stability in the co-simulation of mechanical systems," *Mechanism and Machine Theory*, vol. 131, pp. 172–188, 2019.
- [14] B. Rodríguez, A. J. Rodríguez, B. Sputh, R. Pastorino, M. Á. Naya, and F. González, "Energy-based monitoring and correction to enhance the accuracy and stability of explicit co-simulation," *Multibody System Dynamics*, vol. 55, no. 1, pp. 103–136, 2022.
- [15] C. Gomes, C. Thule, D. Broman, P. G. Larsen, and H. Vangheluwe, "Co-simulation: a survey," *ACM Computing Surveys (CSUR)*, vol. 51, no. 3, pp. 1–33, 2018.
- [16] T. Blochwitz, M. Otter, M. Arnold, C. Bausch, C. Clauß, H. Elmquist, A. Junghanns, J. Mauss, M. Monteiro, T. Neidhold *et al.*, "The functional mockup interface for tool independent exchange of simulation models," in *Proceedings of the 8th international Modelica conference*. Linköping University Press, 2011, pp. 105–114.
- [17] A. Peiret, F. González, J. Kövecses, and M. Teichmann, "Multibody system dynamics interface modelling for stable multirate co-simulation of multiphysics systems," *Mechanism and Machine Theory*, vol. 127, pp. 52–72, 2018.
- [18] X. Dai, A. Raoofian, J. Kövecses, and M. Teichmann, "Model-based co-simulation of flexible mechanical systems with contacts using reduced interface models," *IEEE Robotics and Automation Letters*, vol. 9, no. 1, pp. 239–246, 2023.
- [19] A. Raoofian, X. Dai, and J. Kövecses, "Nonsmooth reduced interface models and their use in co-simulation of mechanical systems," *Journal of Computational and Nonlinear Dynamics*, vol. 19, no. 7, p. 071006, 2024.
- [20] B. Schweizer, P. Li, and D. Lu, "Implicit co-simulation methods: Stability and convergence analysis for solver coupling approaches with algebraic constraints," *ZAMM-Journal of Applied Mathematics and Mechanics/Zeitschrift für Angewandte Mathematik und Mechanik*, vol. 96, no. 8, pp. 986–1012, 2016.
- [21] P. Krus, "Robust modelling using bi-lateral delay lines for high speed simulation of complex systems," in *The International Symposium on Dynamic Problems of Mechanics, March, 13 to 18, 2011 Maresias Beach Hotel São Sebastião, São Paulo, Brazil*, 2011.
- [22] R. Braun, "Multi-threaded distributed system simulations using bi-lateral delay lines," Ph.D. dissertation, Linköpings Universitet (Sweden), 2013.
- [23] R. Braun and D. Fritzon, "Numerically robust co-simulation using transmission line modeling and the functional mock-up interface," *Simulation*, vol. 98, no. 11, pp. 1057–1070, 2022.
- [24] L. Barbierato, S. Steffen-Vogel, D. S. Schiera, E. Pons, L. Bottaccioli, A. Monti, and E. Patti, "Locally distributed digital real-time power system co-simulation via multi-phase distributed transmission line model," *IEEE Transactions on Industry Applications*, vol. 60, no. 6, pp. 8137–8146, 2024.
- [25] J. D. BURTON, K. A. EDGE, and C. R. BURROWS, "Analysis of an electro-hydraulic position control servo-system using transmission-line modelling (tlm)," in *Proceedings of the JFPS International Symposium on Fluid Power*, vol. 1993, no. 2. The Japan Fluid Power System Society, 1993, pp. 507–514.
- [26] R. Braun, R. Hällqvist, and D. Fritzon, "Transmission line modeling co-simulation with distributed delay-size control using steady-state identification," *Engineering with computers*, vol. 40, no. 1, pp. 301–312, 2024.
- [27] E. Celledoni and E. H. Høiseith, "Energy-preserving and passivity-consistent numerical discretization of port-hamiltonian systems," *arXiv preprint arXiv:1706.08621*, 2017.
- [28] H. Parks and M. Leok, "Variational integrators for interconnected lagrange–dirac systems," *Journal of Nonlinear Science*, vol. 27, no. 5, pp. 1399–1434, 2017.
- [29] M. Ehrhardt, M. Günther, and D. Ševčovič, "Structure-preserving coupling and decoupling of port-hamiltonian systems," *arXiv preprint arXiv:2511.20150*, 2025.
- [30] F. J. Argus, C. P. Bradley, and P. J. Hunter, "Theory and implementation of coupled port-hamiltonian continuum and lumped parameter models," *Journal of Elasticity*, vol. 145, no. 1, pp. 339–382, 2021.
- [31] A. Bartel, M. Günther, B. Jacob, and T. Reis, "Operator splitting based dynamic iteration for linear differential-algebraic port-hamiltonian systems," *Numerische Mathematik*, vol. 155, no. 1, pp. 1–34, 2023.
- [32] A. Bartel, M. Diab, A. Frommer, M. Günther, and N. Marheineke, "Splitting techniques for daes with port-hamiltonian applications," *Applied Numerical Mathematics*, vol. 214, pp. 28–53, 2025.
- [33] J. Cervera, A. J. van der Schaft, and A. Baños, "Interconnection of port-hamiltonian systems and composition of dirac structures," *Automatica*, vol. 43, no. 2, pp. 212–225, 2007.
- [34] W. Chen, S. Ran, C. Wu, and B. Jacobson, "Explicit parallel co-simulation approach: analysis and improved coupling method based on h-infinity synthesis," *Multibody System Dynamics*, vol. 52, no. 3, pp. 255–279, 2021.
- [35] H. H. Bauschke and P. L. Combettes, *Convex Analysis and Monotone Operator Theory in Hilbert Spaces*, 2nd ed. Cham: Springer, 2017.
- [36] P.-L. Lions and B. Mercier, "Splitting algorithms for the sum of two nonlinear operators," *SIAM Journal on Numerical Analysis*, vol. 16, no. 6, pp. 964–979, 1979.
- [37] B. F. Svaiter, "On weak convergence of the douglas–rachford method," *SIAM Journal on Control and Optimization*, vol. 49, no. 1, pp. 280–287, 2011.